Green Chemistry

ARTICLE

Solvent-free fabrication of biodegradable all-carbon paper based Field Effect Transistor for human motion detection through strain sensing

Srinivasulu Kanaparthi and Sushmee Badhulika*

There has been a huge demand for low-cost, eco-friendly, flexible and wearable electronics which find applications in personal health monitoring. Flexible electronics based on plastic substrates have been extensively studied in this regard because of their versatility. However, their fabrication involves energy consuming complex procedures and processing of eco-unfriendly materials which limit their use to certain specific applications. Here we report the fabrication of a flexible all-carbon field effect transistor (FET) using a low-cost, recyclable and biodegradable cellulose paper as both substrate as well as dielectric and pencil graphite as source, drain, channel and gate without using any expensive, toxic or non-biodegradable materials. The FET transfer characteristics shows ambipolar behavior which can be utilized in analog electronics applications like rectifier, mixer and frequency multipliers and its mobility was found to be very high compared to reduced graphene oxide based FETs. The FET was utilized as a strain sensor which shows excellent sensitivity for very low strains (of both tensile and compressive type) which is comparable to and even better than recently reported carbon nanotube and graphene based strain sensors. The sensitivity of the FET based strain sensor can be modulated by varying the gate voltage under strain. Furthermore, we investigated the performance of the sensor by integrating it with hand gloves to detect human motion. The results indicate that the sensor can be utilized in patients surveillance in healthcare and human-machine interface (HMI) applications. The successful fabrication of this paper based all-carbon transistor using only paper and pencil graphite and its application in human motion detection using strain sensing indicates that this approach can be used for developing highly scalable, low cost, low energy, flexible electronics for healthcare without using any sophisticated fabrication methods or toxic chemicals.

Introduction

Research in the field of flexible and wearable electronics have gathered significant momentum because of their countless applications in personal healthcare monitoring[1], flexible displays[2], electronic skin[3], energy harvesting devices[4] and microfluidic devices[5]. However, the fabrication of these devices includes complex manufacturing procedures and high end equipment which expend more energy and henceforth constrain their utilization to certain particular applications. Moreover, the plastic and polymer substrates used in flexible electronics take very long time for biodegradation and hence lead to serious environment contamination issues. Therefore, there is a need to develop low cost, versatile and energy efficient fabrication methods with biodegradable substrates to produce flexible electronics which can be used for applications in numerous ranges.

The strong interest in this area has prompted the advancement of flexible paper based devices, for example, UV sensors[6], memory devices[7], touch sensor[8], microfluidic devices[9] and gas sensors[10] using fabrication methods like screen printing and inkjet printing. These printing strategies are exceptionally adaptable to manufacture ease and low energy flexible electronics. However, these solvent based processes involve processing of eco-unfriendly chemicals which result in environment contamination issues, complex steps such as dispersion of sensing material in a special chemical solvent using ultra-sonication or magnetic stirring and usage of toxic surfactant for stabilization of dispersion. It also requires high annealing temperatures or prolonged drying time or washing in order to remove the solvent or surfactant and to improve the electrical conductivity. The synthesis of stable ink with proper rheological properties is also a challenge to get uniform film. Moreover, plasma treatment of substrate is required to improve the wettability and to enhance film adhesion.[11] These pre-deposition and post-deposition treatments and requirements on ink limit the applications of solution based approaches. To address these issues, inexpensive, solvent free fabrication of paper electronics have been demonstrated with multiwalled carbon nanotubes (MWCNT) and graphite composite pellets or pencils.[12,13]

Department of Electrical Engineering, Indian Institute of Technology Hyderabad, Hyderabad, 502285, India. Email: sbadh@iith.ac.in
.

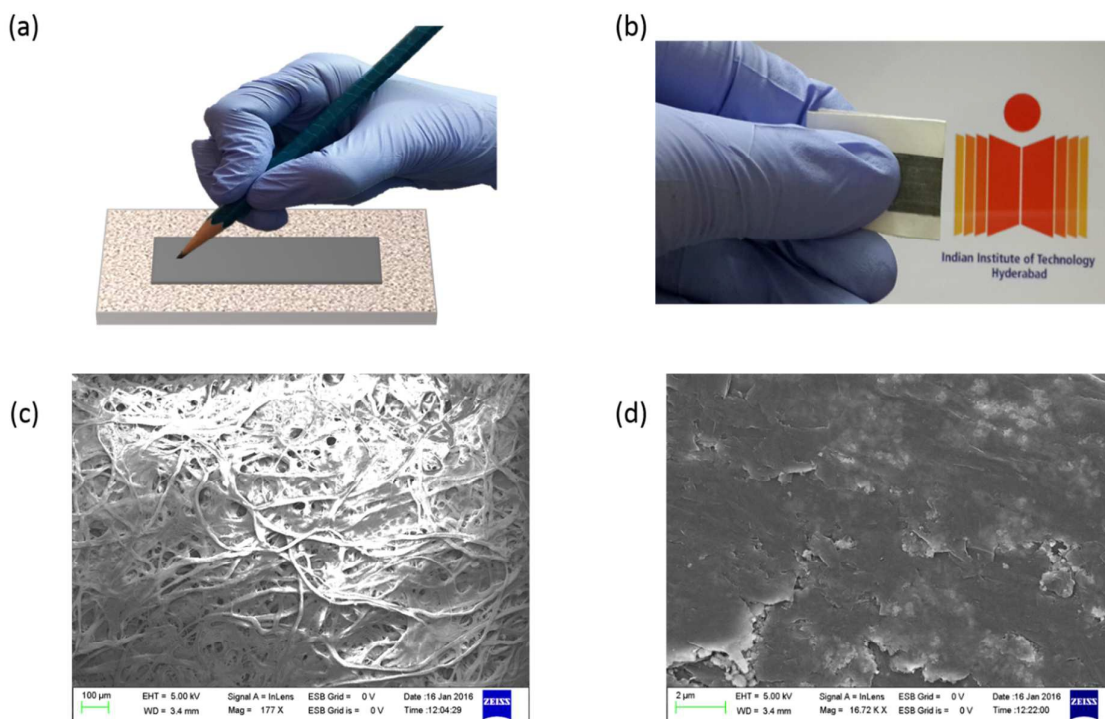However, the materials are either expensive (MWCNT) or carcinogenic (GaSe).

Figure 1: (a) Schematic diagram of fabrication method of pencil on paper device; (b) Photograph of paper based device showing its flexibility; (c) FESEM image of cellulose fiber paper; (d) FESEM image of graphite on paper.

To overcome these shortcomings, commercial pencil graphite on paper approach has been demonstrated in which the devices are fabricated by mechanical abrasion of pencil graphite trace on paper. Supercapacitor[14], chemiresistive gas sensor[15], RC filters[16], strain gauges[15,17] have been successfully developed using pencil graphite trace on paper without using any toxic or expensive materials by simple drawing method. The successful fabrication of these devices uncovers that there is wide scope to develop other low cost, flexible and environment benign sensors and electronic devices using this approach.

In the current study, we report an inexpensive, solvent free, eco-friendly fabrication of all carbon paper field effect transistor (FET) based strain sensor in which the FET is fabricated by using biodegradable cellulose filter paper as both substrate and dielectric and pencil graphite as gate, source, drain and channel. The first paper based back-gate hybrid FET using paper as both substrate as well as gate dielectric was successfully fabricated by Fortunato et al.[18] but involved expensive, energy consuming and sophisticated cleanroom fabrication methods. Recently, Kurra et al. reported the fabrication of paper FET using pencil graphite as channel.[16] However, Ion gel polymer was used as gate dielectric which is non-biodegradable. Ensuring an environmental benign approach, we fabricated all graphite FET which doesn't require any high energy consuming equipment or non-biodegradable materials. The transfer characteristics of the FET are ambipolar in nature and the electron and hole mobilities were found out to be 167 $cm^2V^{-1}s^{-1}$ and 191 $cm^2V^{-1}s^{-1}$ respectively. The strain sensor employed using this FET shows very high sensitivity even at very low strains. It shows a sensitivity of ~37.4% at 1.5 % strain which is higher compared to the recently reported carbon nanotube and graphene based strain sensors. To further demonstrate its utility in a real life scenario, the sensor was integrated with hand gloves to monitor the motion of the fingers. The results indicate that the sensor is very sensitive to the movement of fingers and can be used to monitor human motion at other parts of the body too which can be utilized in healthcare applications such as patients surveillance, health of senior citizens and infants. Moreover, this being a fully solvent free and clean room free fabrication technique enables the device to be used in use-and-throw and use-and-recycle applications where cost is a limitation and laboratory facilities are unavailable. This paper based FET can also be used in applications like frequency multipliers, phase detectors, rectifiers, mixers by utilizing the ambipolar nature of transfer characteristics. To the best of our knowledge, no work has been reported on all carbon paper based FET using only paper as both substrate and dielectric and its application in human motion detection using strain sensing.
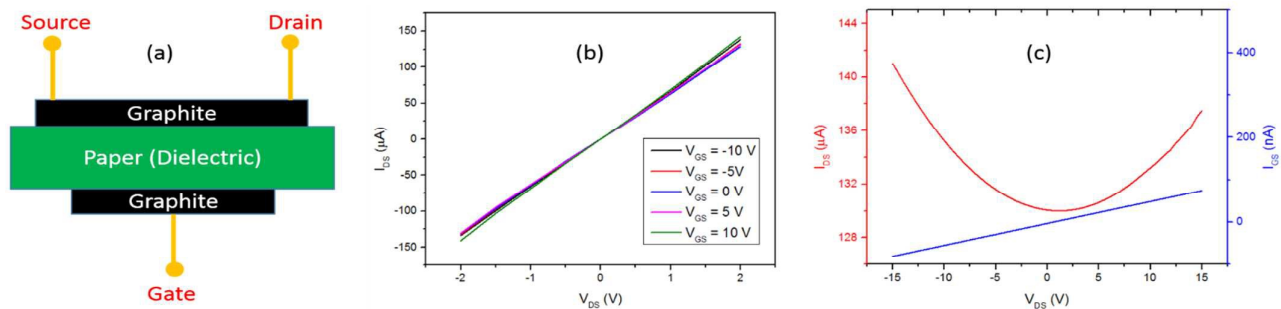
Figure 2: (a) Schematic diagram of all graphite paper field effect transistor; (b) output characteristics of FET; (c) transfer characteristics of FET showing drain current (Red) and leakage current (Blue).

Experimental section

Fabrication of field effect transistor

20 mm length (L) and 10 mm width (W) trace was drawn on both sides of the 120 μm thick cellulose filter paper (EW-81051-92, Advantec, USA) using a graphite pencil (5B grade). The drawing was repeated 10 to 12 times to form a good conductive thin film. One side of the film is used as a gate and the two ends of the other side are used as source and drain. The region between source and drain acts as a channel.

Device characterization

The surface morphology of cellulose filter paper and graphite trace on paper were characterized by a Field Emission Scanning Electron Microscopy (FESEM, supra 40, Carl Zeiss AG). The electrical and electromechanical properties of the FET based sensor were measured by using a semiconductor parameter analyzer (SPA) Agilent b1500a.

Results and discussions

Figure 1(a) illustrates the schematics of pencil graphite based device on a paper substrate. The device was fabricated by simple mechanical abrasion of 5B grade soft pencil on filter paper. The 5B

pencil was preferred to draw the trace because it has more graphite content (82%) and more conductive compared to HB, H series and other lower B series pencils [40]. The friction between pencil lead and rough surface of the paper ensures the deposition of large graphite chunks while drawing pencil traces on paper. The as fabricated device is mechanically stable, flexible and hence wearable as shown in figure 1(b). The SEM image of paper reveals the randomly oriented cellulose fibers network and porosity of the paper as shown in figure 1(c). The roughness of the paper surface ensures continuous deposition of conductive graphite thin film on paper as shown in figure 1(d) which provides sufficient adsorption area required for electrical double layer formation when used as gate dielectric.

The graphite pencil trace on a paper device fabricated as a back gate all-carbon field effect transistor in which cellulose paper acts as a substrate as well as a dielectric and the pencil graphite acts as the gate, source, drain and the channel is illustrated in figure 2(a). The performance of all-carbon paper field effect transistor was assessed by electrical characterization in air at room temperature. The output characteristics in figure 2(b) shows that the conductance increases with increase in gate voltage and shows perfectly ohmic behaviour, which is a characteristic of zero band gap material. Transfer characteristics of FET in figure 2(c) shows ambipolar behavior consistent with the semimetallic nature of graphite[34-37], with a positive charge neutrality point (Dirac point) at ~ 1V. This shift in charge neutrality point from 0 V is
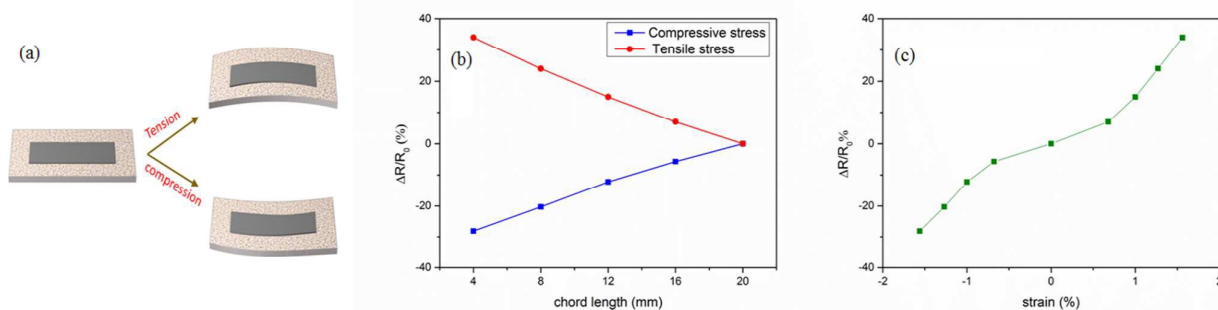

Figure 3: (a) Schematic illustrating tension and compression; (b) relative change in resistance with tension and compression as a function of chord length; (c) relative change in resistance with tension and compression as a function of strain.

because of the imperfections in graphite, unexpected doping of water molecules present in the surrounding humid atmosphere and the impurities present in the pencil graphite.[19,20] Besides, the asymmetry in transfer characteristics on both sides of charge neutrality point might be credited to the fortuitous doping of pencil trace by oxygen molecules present in the surrounding medium which suppresses the electron mobility of the graphite channel and hence the electron and hole mobilities are unequal.[21] The resistance of the channel depends on the mobility and the difference between gate source voltage and charge neutrality point V_{cn}.[30]

$$R_{ch} = R_{con} + \left(L/Wnq\mu(V_{GS} - V_{cn}) \right)$$

where R_{con} is the contact resistance between source/drain and channel which is negligible as it is all carbon transistor in which source/drain and channel have same material. As the mobility and $(V_{GS} - V_{cn})$ are slightly different for V_{GS} =-10 V and V_{GS} = 10 V, the line corresponding to V_{GS} =-10 V will not coincide with the line corresponding to V_{GS} = 10 V as shown in figure 2(b). Similarly the line corresponding to Vgs = -5 V and Vgs =5 V are also different but visually not distinguishable as the difference is very low. The gate leakage current increases linearly with the gate voltage and is three orders lower in magnitude compared to the channel current as illustrated in figure 2(c). These results indicate that paper as a gate dielectric is effective in deriving electric field from pencil trace because the graphite on paper forms an electrochemical double layer.[14,22] The FET showed electron (hole) mobility µ of 167 (191) cm^2/V.s, calculated from gate capacitance model and the linear regime of transfer curve according to

$$\mu = \left(L/WCV_{DS} \right)\left(dI_{DS}/dV_{GS} \right),$$

where C is the capacitance per unit area, W (10 mm) and L (20 mm) are the channel width and length respectively. The extracted mobility values from transfer characteristics of multiple devices show +/- 10 % variation from these values which may be due to the roughness of the paper and non-uniform pencil graphite film revealed by atomic force microscopy (AFM) images of graphite pencil trace on paper (as shown in Supporting Information, Figure S1). The mobility values obtained in this experiment are comparable to the mobility of FET on paper in which pencil trace as channel and ion gel as dielectric[16,23] and lesser compared to the graphite on SiO$_2$ FET[19] but higher compared to organic FETs[38,39,42] and reduced graphene oxide (rgo) based FETs.[24,41]

Graphite FET on a paper is exploited as a strain sensor with zero gate voltage as shown in Figure 3(a). The strain sensor works on the principle of microcontact reversible effect of graphite film on paper.[17] The conductance of the graphite film depends on the contacts between graphite nanosheets. The resistance of the strain sensor can be reproduced reversibly by separating and overlapping of graphite nanosheets on the paper. The sensor encounters tensile stress when it twists outwards and the cellulose fibers on the paper expands. Hence, cracks occurs inside the graphite film on the paper due to separation of the graphite nanosheets, which leads to decrease in the conductance of the strain sensor. Similarly, the sensor encounters compressive stress when it twists inwards and the graphite nanosheets overlap each other, thereby increasing the conductance of the sensor. The performance of the strain sensor was evaluated by measuring the relative change in resistance of the sensor under tensile and compressive stress by twisting the sensor outwards and inwards respectively as a function of chord length and applied strain. The resistance of the sensor increases (decreases) with
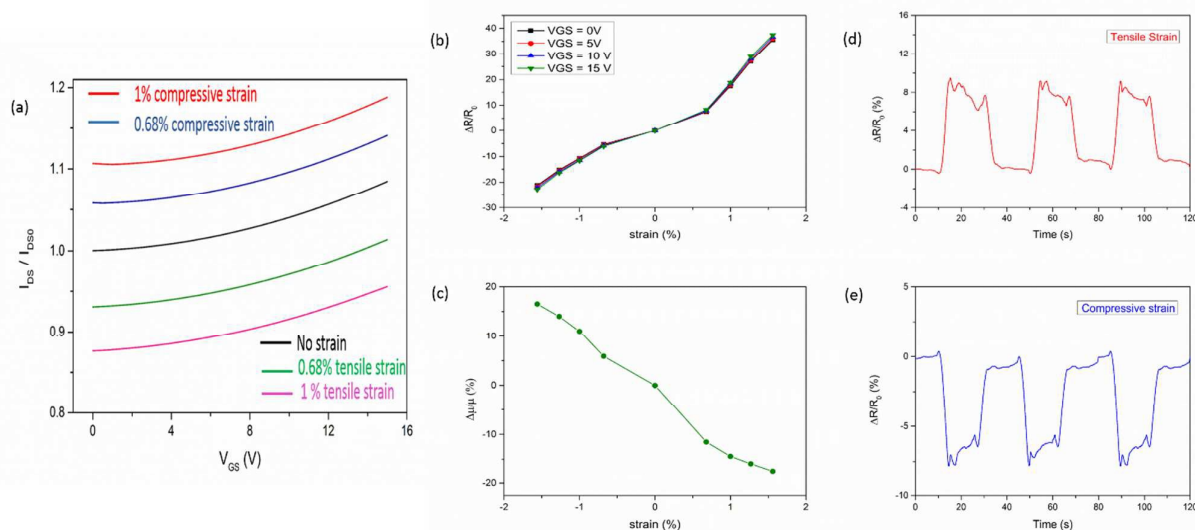

Figure 4: (a) Transfer characteristic of FET under tensile and compressive strains; (b) relative change in resistance with strain at different gate voltages ; (c) relative change in mobility of FET with strain ; (d) temporal characteristics of FET under tension; (e) temporal characteristics of FET under compression (V_{GS} = 5V and V_{DS}=2V).

the decrease in the chord length under tensile (compressive) stress as shown in figure (3b). Therefore the bending or twisting direction can be identified by the sign of the change in the resistance of the strain sensor. The chord length c of the strain sensor is related to the radius of the curvature r by the relation c = 2r*sin $(l/2r)$, where l is the length and r is the radius of the arc of the sensor under tensile or compressive stress. The strain of the sensor Ɛ can be evaluated by using the relation Ɛ = +/- (h/r), where h (~120 μm) is the thickness of the sensor. The strain of the sensor is calculated from the above expression and the relative change in resistance as a function of the strain under tension and compression is plotted as shown in figure 3(c). The negative and positive portions of the strain represents the compressive and tensile stress respectively. The sensitivity or gauge factor is given by the relation GF = $(\Delta R/R_0)/Ɛ$. It was found that the sensitivity of the sensor under compressive stress is lower compared to that of the sensor under tensile stress which is due to cracks present in the film. The sensitivity or gauge factor is lower for smaller strains because of smaller cracks between graphite slices or smaller overlapping area between adjacent graphite nanosheets under tension or compression respectively. Similarly, the sensitivity is higher for larger strains because of larger cracks or larger overlapping area between adjacent graphite nanosheets under stress. The sensor shows a sensitivity of 12 to 20% (with the strain range from -1.5% to 1.5%) which is comparable and even higher compared to recently reported graphene and carbon nanotube strain sensors.[1, 25, 26]

The performance of the FET based strain sensor was evaluated by applying a gate voltage from 0 to 15V. The normalized transfer characteristics of the FET based strain sensor under both tensile and compressive stress are shown in figure 4(a). It was observed that the drain current increases with the increase in compressive strain and decreases with increase in tensile strain. The relative change in resistance with strain and

hence sensitivity or gauge factor GF increases with both compressive and tensile stress as shown in figure 4(b) due to the modulation of channel current with the gate voltage. It was found that the sensitivity improved by 5.4% to 14.6 % by applying a gate voltage of 15V in the strain range of -1.5% to 1.5 %. The sensor exhibited a sensitivity of 37.4% at 1.5% strain and a gate voltage of 15 V as against 35.5% with 0 V gate voltage. The mobility of the electron increases with the compressive strain and decreases with tensile strain. This variation in field effect mobility μ_{FE} can be understood by Matthiessen's rule represented by the equation (1) and (2)

$$1/\mu FE = 1/\mu int + 1/\mu ext \qquad (1)$$
$$1/\mu ext = 1/\mu PB + 1/\mu CI + 1/\mu SR + 1/\mu SPP \qquad (2)$$

Where μ_{int} is the mobility controlled by internal scattering and μ_{ext} is the mobility controlled by external scattering arises from scattering of coulomb impurities (μ_{CI}), surface roughness (μ_{SR}) and dielectric surface polar phonon (μ_{SPP}) and scattering at potential barrier (μ_{PB}).[27,28] The change in carrier mobility constrained by other scattering phenomenon is negligible compared to the change in mobility constrained by scattering at potential barrier (μ_{PB}).[28] The coupling between neighboring graphite nanosheets in the channel influences the level of overlapping and the separation between graphite sheets at the intersection and also determines the potential barrier height which affects the scattering at barrier.[29] The width of the boundary between adjacent graphite nanosheets determines the transport properties of graphite channel. The carrier transport in the channel is due to two mechanisms namely tunnelling and thermionic emission [31]. The charge carriers with less energy compared to the potential barrier height will tunnel through the barrier or boundary between the nanosheets provided the width of the boundary is sufficiently small. The charge carriers which have sufficient energy to cross over the energy barrier or potential barrier will cross over the barrier. This is called thermionic emission. Tunnelling current is directly proportional to the tunnelling distance or width of the barrier. Moreover, the height of
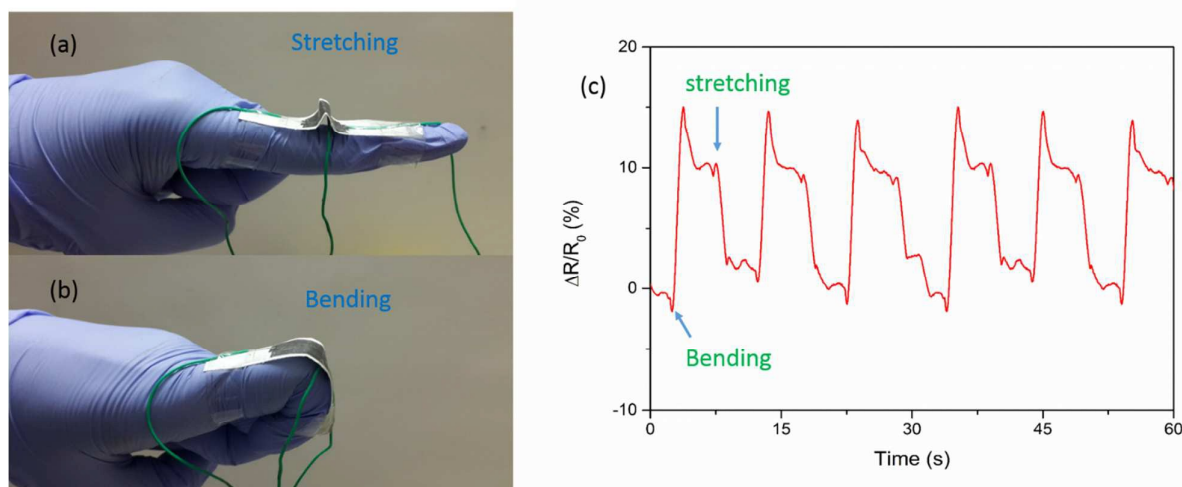

Figure 5: (a),(b) Photographs of wearable FET based strain sensors attached to fore-finger for human motion detection; (c) relative change in resistance of the sensor with bending (V_{GS} =5V and V_{DS} = 2V) considering the resistance in stretched condition as reference.

the potential barrier is also directly proportional to the potential barrier width or the boundary width between the individual graphite sheets. Under compressive strain, the separation or the width of the boundary between the adjacent graphite nanosheets decreases. Therefore the tunnelling distance decreases with compressive strain. In addition to this the potential barrier height decreases as it is directly proportional to the boundary width. The decrease in potential barrier height results in higher mobility μ_{PB} of charge carriers due to reduced scattering. The resistance of the channel is proportional to the potential barrier height and the tunnelling distance between graphite sheets as given by

$$R \propto exp(\beta x)$$

where β is a function of barrier height and x is the width of the boundary or tunnelling distance between graphite sheets.[32,33] Therefore the resistance decreases with the compressive strain as potential barrier height and tunnelling distance decreases with compressive strain In contrast, the separation or the width of the boundary between adjacent graphite sheets increases upon tensile strain which results in increase in tunnelling distance and potential barrier height. Therefore the mobility decreases as a result of enhance scattering due to increase in barrier height and resistance increases due to increase in both barrier height and tunnelling distance. The relative change in mobility of the electron as a function of strain is plotted as shown in figure 4(c). The drain current is proportional to the mobility of charge carriers and the gate voltage at a constant drain voltages as given by the following equation

$$I_{DS} \propto 1 \Big/ \left(R_{con} + \left(L \Big/ Wnq\mu(V_{GS} - V_{cn})\right)\right)$$

Under compressive strain, the drain current increases as a result of increase in the mobility of charge carriers. Similarly, the drain current decreases upon tensile strain as a result of decrease in mobility of the charge carriers as shown in figure 4(a). These results are consistent with that of reduced graphene oxide FET under stress.[28]

Further we tested the reliability of the sensor by bending and stretching multiple times with small strain of 0.68 % at V_{DS}=2V and V_{GS}=5V. The results plotted as shown in figure 4(d) and figure 4(e) represents the relative change in resistance with time under tensile and compressive strain of 0.68%. These results reveal that the sensor is mechanically robust and reliable.

As a proof of concept, the strain sensor was utilized for detecting human motion which can find applications in robotics, human machine interfacing (HMI) and healthcare monitoring. The strain sensor was attached to the fore-finger as shown in figure 5(a) and 5(b) and the gate voltage and drain voltage of the FET based sensor are 5V and 2V respectively. The relative change in resistance as a function of time with bending and stretching of finger is as shown in figure 5(c). The

change in resistance is caused by tensile stress with bending of finger and it is due to both tensile stress and compressive stress with stretching of finger. The device performance was tested after several bending cycles and after 20 days of fabrication. The results were reproducible presenting good stability. These results indicate that the strain sensor can be used to monitor personal healthcare by integrating it at various parts of the human body as well as in robotics and human machine interface (HMI) applications.

Conclusions

In summary, we report fabrication of a low cost, low energy, flexible, eco-friendly and solution-free all carbon field effect transistor with cellulose paper as both substrate and dielectric and pencil graphite as gate, source, drain and channel without using elaborate procedures, sophisticated instruments and/or toxic chemicals. The FET was used to demonstrate human motion detection using strain sensing and it exhibited very high sensitivity to finger movements when integrated with hand gloves. It was observed that the sensor's performance is reproducible and stable over the time. The successful fabrication of this durable, paper based FET and its utilization in human motion detection indicates that it is feasible to fabricate biodegradable paper based eco-friendly, efficient, flexible and wearable electronics which find numerous potential applications in healthcare, robotics and human-machine interface (HMI).

Acknowledgements

Notes and references

1   T. Yamada, Y. Hayamizu, Y. Yamamoto, Y. Yomogida, A. Izadi-Najafabadi, D. N. Futaba and K. Hata, *Nat. Nanotechnol.*, 2011, 6, 296–301.
2   M. S. White, M. Kaltenbrunner, E. D. Głowacki, K. Gutnichenko, G. Kettlgruber, I. Graz, S. Aazou, C. Ulbricht, D. A. Egbe, M. C. Miron and Z. Major, *Nat. Photonics.*, 2013, 7(10), 811-816.
3   M. L. Hammock, A. Chortos, B. C. K. Tee, J. B. H. Tok and Z. N. Bao, *Adv. Mater.*, 2013, 25, 5997–6037.
4   Q. Liao, Z. Zhang, X. H. Zhang, M. Mohr, Y. Zhang, H.-J. Fecht, *Nano Res.,* 2014, *7, 917–928.*
5   H. Ko, J. Lee, Y. Kim, B. Lee, C. H. Jung, J. H. Choi, O. S. Kwon and K. Shin, *Adv. Mater.,* 2014, 26(15), 2335-2340.
6   K. ul Hasan, O. Nur and M. Willander, *Appl. Phys. Lett.*, 2012, 100(21), 211104.
7   D. H. Lien, Z. K. Kao, T. H. Huang, Y. C. Liao, S. C. Lee and J. H. He, *ACS nano.*, 2014, 8(8), 7613-7619.
8   R. Z. Li, A. Hu, T. Zhang and K. D. Oakes, *ACS. Appl. Mater. Inter.,* 2014, 6(23), 21721-21729.
9   M. M. Mentele, J. Cunningham, K. Koehler, J. Volckens and C. S. Henry, *Anal. Chem.,* 2012, 84(10), 4474-4480.
10 J. Zhang, L. Huang, Y. Lin, L. Chen, Z. Zeng, L. Shen, Q. Chen and W. Shi, *Appl. Phys. Lett.*, 2015, 106(14), 143101.

11 K. Y. Shin, J. Y. Hong and J. Jang, *Adv. Mater.*, 2011, 23(18), 2113-2118.

12 K. M. Frazier, K. A. Mirica, J. J. Walish and T. M. Swager, *Lab. Chip.*, 2014, 14(20), 4059-4066.

13 V.V. Brus, P. D. Maryanchuk, Z. D. Kovalyuk and S. L. Abashyn, *Nanotechnology*, 2015, 26(25), 255501.

14 G. Zheng, L. Hu, H. Wu, X. Xie and Y. Cui, *Energ. Environ. Sci.,* 2011, 4(9), 3368-3373.

15 C. W. Lin, Z. Zhao, J Kim and J. Huang, *Sci. Rep.,* 2014, 4, 3812.

16 N. Kurra, D. Dutta and G. U. Kulkarni, *Phys. Chem. Chem. Phys.,* 2013, 15(21), 8367-8372.

17 X. Liao, Q. Liao, X. Yan, Q. Liang, H. Si, M. Li, H. Wu, S. Cao and Y. Zhang, *Adv. Funct. Mater.*, 2015, 25(16), 2395-2401.

18 E. Fortunato, N. Correia, P. Barquinha, L. Pereira, G. Gonçalves and R. Martins, *IEEE. Electr. Device. L.,* 2008, 29(9), 988-990.

19 A. Sagar, K. Balasubramanian, M. Burghard and K. Kern, Appl. Phys. Lett., 2012, 100, 203116.

20 H. Xu, Y. Chen, J. Zhang and H. Zhang, *Small*, 2012, 8(18), 2833-2840.

21 I. Silvestre, E. A. de Morais, A. O. Melo, L.C. Campos, A. M. B. Goncalves, A. R. Cadore, A. S. Ferlauto, H. Chacham, M. S. Mazzoni and R. G. Lacerda, *ACS nano*, 2013, 7(8), 6597-6604.

22 D. Gaspar, S. N. Fernandes, A. G. De Oliveira, J.G. Fernandes, P. Grey, R. V. Pontes, L. Pereira, R. Martins, M. H. Godinho and E. Fortunato, *Nanotechnology*, 2014, 25(9), 094008.

23 S. Mandal, R. K. Arun, N. Chanda, S. Das, P. Agarwal, J. Akhtar and P. Mishra, *J. Electr. Mater.*, 2015, 44(1), 6-12.

24 B. J. Kim, M. S. Kang, V. H. Pham, T. V. Cuong, E. J. Kim, J. S. Chung, S. H. Hur and J. H. Cho, *J. Mater. Chem*., 2011, 21(34), 13068-13073.

25 E. Roh, B.U. Hwang, D. Kim, B.Y. Kim and N.E. Lee, *ACS nano*, 2015, 9, 6252-6261.

26 J. J. Park, W. J. Hyun, S. C. Mun, Y. T. Park and O. O. Park, *ACS Appl. Mater. Inter.*, 2015, 7(11), 6317-6324.

27 Z. Liu, A. A. Bol, W. L. Haensch, *Nano Lett.,* 2010, 11(2), 523-528.

28 T. Q. Trung, N. T. Tien, D. Kim, M. Jang, O. J. Yoon and N.E. Lee, *Adv. Func. Mater.*, 2014, 24, 117-124.

29 E. S. Snow, J. P. Novak, P. M. Campbell and D. Park, *Appl. Phys. Lett*., 2003, 82(13), 2145-2147.

30 Z. Zhang, H. Xu, H. Zhong, and L. M. Peng, *Appl. Phys. Lett.*, 2012, 101(21), 213103.

31 T. Dinh, H. P. Phan, D. V. Dao, P. Woodfield, A. Qamar and N. T. Nguyen, *J. Mater. Chem. C,* 2015, 3, 8776-8779.

32 T. K. Kang, *Appl. Phys. Lett*., 2014, 104, 073117.

33 J. Zhao, C. He, R. Yang, Z. Shi, M. Cheng, W. Yang, G. Xie, D. Wang, D. Shi and G. Zhang, *Appl. Phys. Lett.*, 2012, 101, 063112.

34 K. Lee, J. Park, M. S. Lee, J. Kim, B. G. Hyun, D. J. Kang, K. Na, C. Y. Lee, F. Bien and J. U. Park, *Nano let.*, 2014, 14(5), 2647-2654.

35 J. U. Park, S. Nam, M. S. Lee, and C. M. Lieber, *Nat. Mater.*, 2012, 11(2), 120-125.

36 Q. He, S. Wu, S. Gao, X. Cao, Z. Yin, H. Li, P. Chen and H. Zhang, *ACS nano*, 2011, 5(6), 5038-5044.

37 W. Chen, Y. Yu, X. Zheng, S. Qin, F. Wang, J. Fang, G. Wang, C. Wang, L. Wang, G. Peng and X. A. Zhang, *Sci. Rep.*, 2015, *5*, 12198.

38 M. X. Zhang, S. Chai and G. J. Zhao, *Org. Electron.*, 2012, 13(2), 215-221.

39 M. X. Zhang and G. J. Zhao, ChemSusChem, 2012, 5, 879 – 887.

40 M. C. Sousa and J. W. Buchanan, *Comput. Graph. Forum,* 2000, 19, 27.

41 G. Eda, G. Fanchini and M. Chhowalla, *Nat. Nanotechnol.*, 2008, *3*(5), 270-274.

42 Y. Chen, Y. Xu, K. Zhao, X. Wan, J. Deng and W. Yan, *Nano Res.*, 2010, 3(10), 714-721.
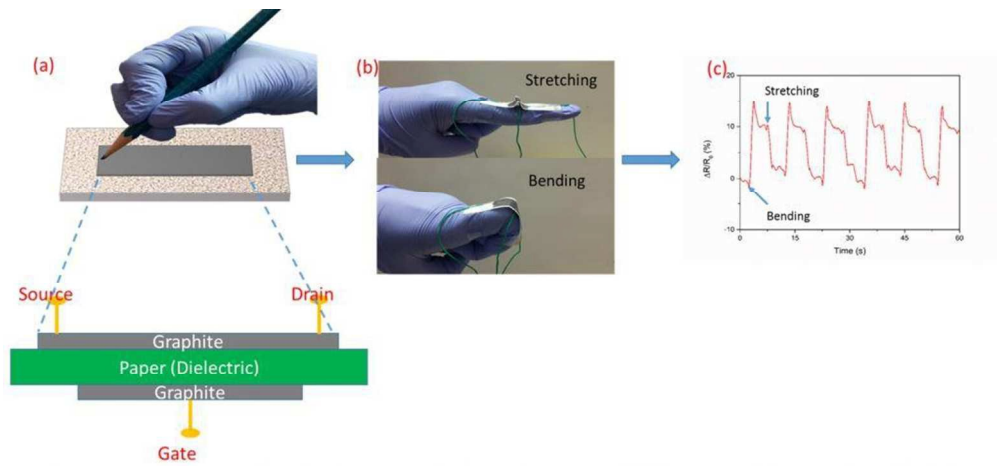
(a) Schematic diagram of fabrication method of pencil on paper FET device; (b)Image of the flexible and wearable FET based strain sensors attached to fore-finger for human motion detection;(c) strain sensing considering the resistance in stretched condition as reference.

173x94mm (150 x 150 DPI)